Influence of a Dense, Low-height Shrub Species on the Accuracy of a Lidar-derived DEM

Samuel B. Gould, Nancy F. Glenn, Temuulen T. Sankey, and James P. McNamara

Abstract

Airborne lidar provides an effective platform for collecting elevation data. However, the accuracy of lidar-derived digital elevation models (DEMs) can be adversely affected by natural conditions as well as methods used to process the data. Using a lidar dataset from a mountainous region of southwest Idaho, this study extends previous assessments of DEM accuracy with a focused investigation of a specific dense, low-height shrub species (Ceanothus velutinus). Bare-earth elevations were collected using survey-grade GPS and compared to lidar-derived elevations to assess DEM accuracy. Results suggest that the magnitude of elevation error varied depending on morphological characteristics of ceanothus, terrain slope, and filtering parameters used to process the lidar data. When using optimal filtering parameters, root mean square error ($RMSE_Z$) was largest in areas of ceanothus cover, ranging from 0.17 to 0.26 m in slopes $<25°$ and 0.28 to 0.37 m in slopes $\geq 25°$. An examination of lidar returns found that ceanothus obstructed laser pulse penetration and few returns reached the ground surface. In areas of ceanothus cover, we conclude that the obstruction of the ground surface contributed to filtering errors, which resulted in mislabeled ground returns and decreased accuracy in bare-earth DEMs. These results have implications for the use of lidar-derived DEMs in areas of ceanothus throughout western North America, and in ecosystems with similar dense shrub cover.

Introduction and Background

Airborne laser scanning, also referred to as lidar (Light Detection and Ranging), is an active remote sensing technology capable of collecting detailed three-dimensional information about the Earth's surface. Small-footprint, discrete-return systems have the ability to penetrate surface vegetation and yield multiple returns from the canopy and underlying terrain. The dense collection of elevation data makes lidar an attractive data source for the production of high-resolution digital elevation models (DEMs) used in many geographic information system (GIS) applications. While the vertical accuracy of many lidar systems is commonly quoted as ~0.15 m (Baltsavias, 1999), such accuracy is typically only achievable under the most ideal circumstances (Hodgson and Bresnahan, 2004). Several studies (Reutebuch *et al.*, 2003; Hodgson and Bresnahan, 2004; Su and Bork, 2006; Raber *et al.*, 2007; Bater and Coops, 2009; Spaete *et al.*, 2011) have analyzed the accuracy of lidar-derived DEMs and found natural conditions such as land-cover and terrain slope, as well as lidar point processing, to be significant influential factors on accuracy.

Previous studies investigating the influence of land-cover (Hodgson *et al.*, 2003; Su and Bork, 2006) have categorized vegetation according to similar characteristics (e.g., low grass, high grass, shrub, coniferous, deciduous, etc.), which provide generalized error predictions, but may overlook unique interactions between the laser beam and a particular species of vegetation. Analyzing error within specific types of vegetation is necessary to understand and quantify the accuracy of lidar-derived ground surfaces in semiarid mountainous ecosystems, where dense, broadleaf shrubs coincide with sparse shrub-steppe and mixed-forest communities.

Morphological characteristics of vegetation such as ceanothus (*Ceanothus velutinus*) present unique challenges for the accurate generation of DEMs using lidar data. Few openings in the canopy are large enough for lidar pulses (~0.20 m diameter) to pass through and the oval-shaped, waxy texture of the leaves (Figure 1) highly reflect and attenuate laser beam irradiance. As a result, the dense stand characteristics and leaf orientation of ceanothus can prevent lidar pulses from reaching the ground surface, which potentially leads to mistakenly-labeled ground returns and subsequent error in DEM elevations. Low-height vegetation can also be problematic because of the small elevation differences between the top of the vegetation and underlying ground surface. Two lidar echoes can only be discriminated if their distance is larger than half of the pulse length (Beraldin, 2010), which is commonly on the order of 3 to 6 ns or 1 to 2 m (Liu, 2008). As a consequence, the reflected energy of a pulse from the vegetation becomes comingled with the reflected energy from the ground surface, and the system is unable to discern more than one return in short vegetation (Schmid *et al.*, 2011).

A well-documented characteristic of observed elevation error in lidar data is the relationship with terrain slope (Maling 1989). As slope increases, "apparent" error may also increase due to horizontal error in the lidar observation. Spaete *et al.* (2011) examined the effects of slope and vegetation on the accuracy of a lidar-derived DEM and calculated potential vertical error (PVE) using the average slope for each of their vegetation categories. They found a low PVE (0.026-0.037 m) in slopes $<10°$ and a higher PVE (0.075 to 0.12 m) in slopes $>10°$. Root mean square error ($RMSE_Z$) values for slopes $>10°$ were roughly twice than those for slopes $<10°$, suggesting that PVE likely contributed to the overall $RMSE_Z$. Hodgson and Bresnahan (2004) and Su and Bork (2006), respectively,

Samuel B. Gould, Nancy F. Glenn, Temuulen T. Sankey, and Lucas P. Spaete are with the Department of Geosciences, Boise Center Aerospace Laboratory, Idaho State University, 322 E. Front Street, Boise, ID 83702 (goulsamu@isu.edu).

James P. McNamara is with the Department of Geosciences, Boise State University, 1910 University Drive, Boise, ID 83725.
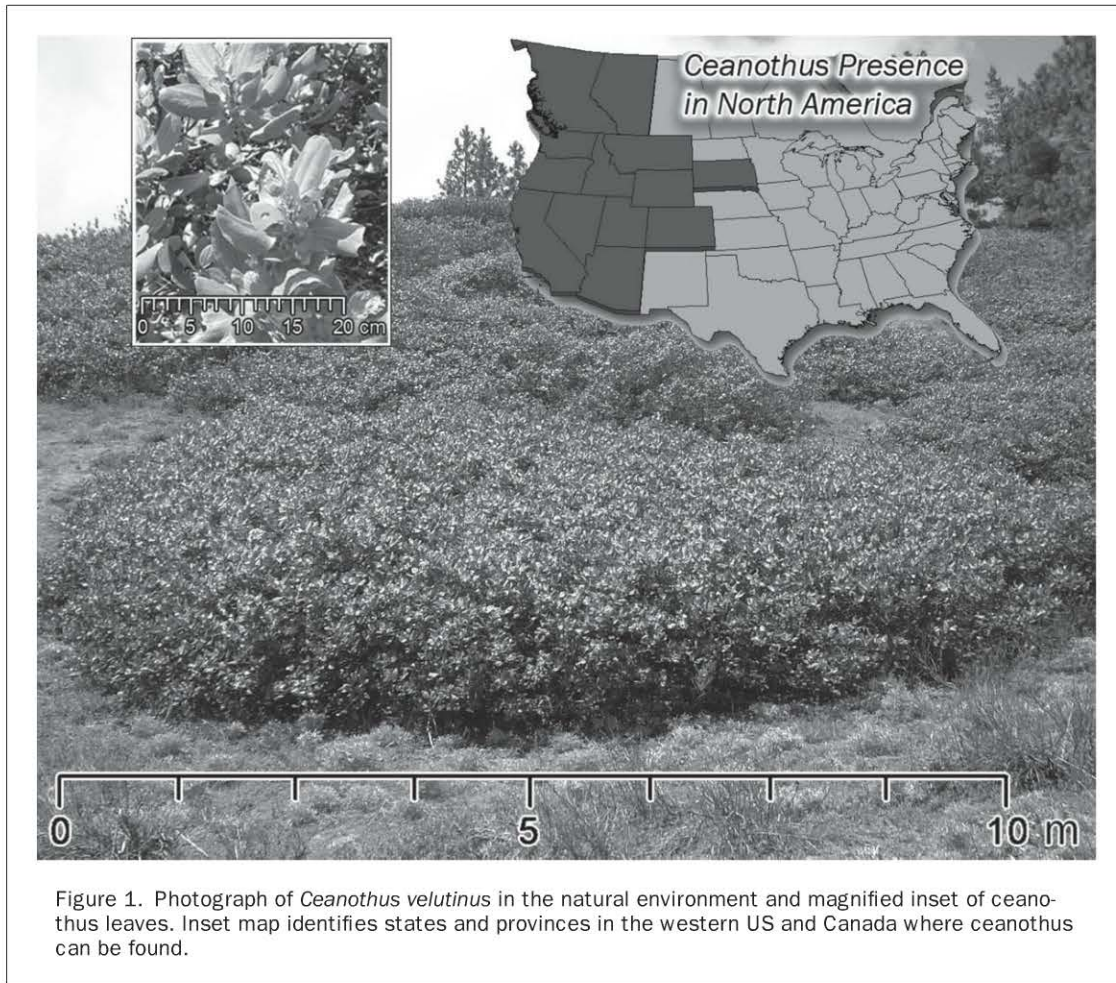
Figure 1. Photograph of *Ceanothus velutinus* in the natural environment and magnified inset of ceanothus leaves. Inset map identifies states and provinces in the western US and Canada where ceanothus can be found.

found similar results, with $RMSE_Z$ on slopes >25° twice those found on relatively flat areas and $RMSE_Z$ of slopes >10° twice those found on slopes <2°.

In nearly all lidar applications, height-filtering of the 3D point cloud is a necessary process to determine which lidar returns are from the ground surface and which are from non-ground features. Classifying the lidar data is a critical step for DEM generation, but the development of methods to accurately separate returns has proven to be difficult. A common assumption of many height-filtering algorithms is that the lowest return in a specified neighborhood represents the ground surface (Meng *et al.*, 2010). This method can be problematic in areas of complex vegetation and varying topography where the lowest return may not truly represent the ground surface. Many filtering algorithms have been proposed with none performing equally well for all landscapes (Forlani and Nardinocchi, 2007). Thus, an understanding of the filtering method used and its ability to accurately separate returns within specific vegetation and varying terrain is necessary for a viable DEM accuracy assessment. Several studies (Glenn *et al.*, 2011; Mitchell *et al.*, 2011; Sankey and Bond, 2011; Spaete *et al.*, 2011) have used the same height-filtering method as implemented in this research determining optimal parameters based on study-specific accuracy.

Although previous studies have examined the accuracy of lidar-derived DEMs across varying terrain and land cover (Reutebuch *et al.*, 2003; Hodgson and Bresnahan, 2004; Bater and Coops, 2009; Spaete *et al.*, 2011), relatively few have focused on quantifying the error for an individual species of vegetation (Su and Bork, 2006). Furthermore, little research has investigated the effects in semiarid mountainous landscapes where complex topography (slopes >25°) and dense, low-height shrubs are abundant. Our study investigated the influence of ceanothus (*Ceanothus velutinus*), a native broadleaf evergreen shrub, on the accuracy of a lidar-derived DEM. With populations of ceanothus found in several mountainous ecosystems throughout the western US and Canada (Figure 1), such an investigation has important implications for lidar applications at a regional scale. This investigation may also hold relevance for ecosystems where similar but unrelated species of vegetation exist and interact with lidar in much the same manner. The objectives of this study were to: (a) determine if ceanothus introduces elevation error in derived DEMs, (b) quantify the vertical accuracy for derived DEMs within combinations of ceanothus cover and terrain slope, (c) explore the influence of filtering parameters on DEM accuracy, and (d) determine lidar pulse penetration by analyzing the vertical distribution of returns within ceanothus canopy.

Methods

Study Area

This study was conducted in the Dry Creek Experimental Watershed (DCEW) located approximately 16 km northeast of the city of Boise in the semiarid region of southwest Idaho (Figure 2). Roughly 27 km² in area, DCEW contains complex mountainous and foothills topography. The terrain is highly variable with an average slope of ~14°, characterized by steep slopes on both the north- and south-facing aspects, converging in a narrow valley-bottom (McNamara *et al.*, 2005). Elevations range from 1,000 m at the southern outlet of Dry Creek to 2,100 m at the northern headwaters (Aishlin *et al.*, 2011; McNamara *et al.*, 2005). Lower regions of the watershed are classified as steppe summer dry climate (annual precipitation ~37 cm); while the upper portion of the watershed is classified as moist continental climate with dry summers (annual precipitation ~57 cm). Vegetation varies with elevation, geology, microclimate, soil type, and topography. At lower elevations, grasses and shrubs dominate, with cottonwoods (*Populus deltoid*) and ponderosa pine (*Pinus ponderosa*) lining the fluvial channels. Upper elevations are dominated by ponderosa pine and Douglas-fir (*Pseudotsuga menziesii*) with patches of lodgepole pine (*Pinus contorta*) and aspen (*Populus tremuloides*). Middle elevations range from grasses and shrubs to open forest communities, functioning as an ecotonal zone between the sagebrush- (*Artemisia* spp.) and grass-dominated lowlands and more densely forested uplands (Shallcross, 2011).

Ceanothus distribution and terrain slope were both considered when selecting a suitable study area. Terrain slope was analyzed for the entire watershed, and categorized using a lidar-derived slope map. Qualitative, pre-survey analysis identified probable areas of ceanothus within the mid- to upper-watershed (~1500-2000 m in elevation) using a combination of aerial imagery (National Agriculture Imagery Program, 2009) and a lidar-derived vegetation-height raster. Field-collection was then focused within the study area, and specific sampling areas were randomly selected in the field (Figure 2).

Target Species: *Ceanothus velutinus*

This study assumed that ceanothus in our study area exhibited negligible change in the time between the lidar data acquisition (November 2007) and the field data collection (June 2011). Ceanothus is a slow-growing species, with population growth in similar environments following a sigmoid curve, reaching an equilibrium growth stage between the ages of 10 to 15 years (Zavitkovski and Newton, 1968). Limited samples of shrub age estimates at the study area using annual growth rings indicated that the sampled populations of ceanothus were likely within the equilibrium growth stage and no recorded history of fires have occurred in the study area within the last century. Ceanothus is also classified as an evergreen shrub, so it maintains its leaves throughout the year indicating that minimal differences would be found due to seasonal changes.

Lidar Data Acquisition

Small-footprint, discrete-return lidar data were acquired during November 2007 for the entire DCEW as part of a larger collection of the Owyhee Uplands. Data were collected using a Leica ALS50 Phase II laser sensor (Leica Geosystems, Heerbrugg, Switzerland), mounted in a Cessna Caravan 208B flown approximately 900 m above ground level (AGL). The sensor utilizes a scanning mechanism which was set to a maximum scan angle of ±14° off nadir and capable of collecting
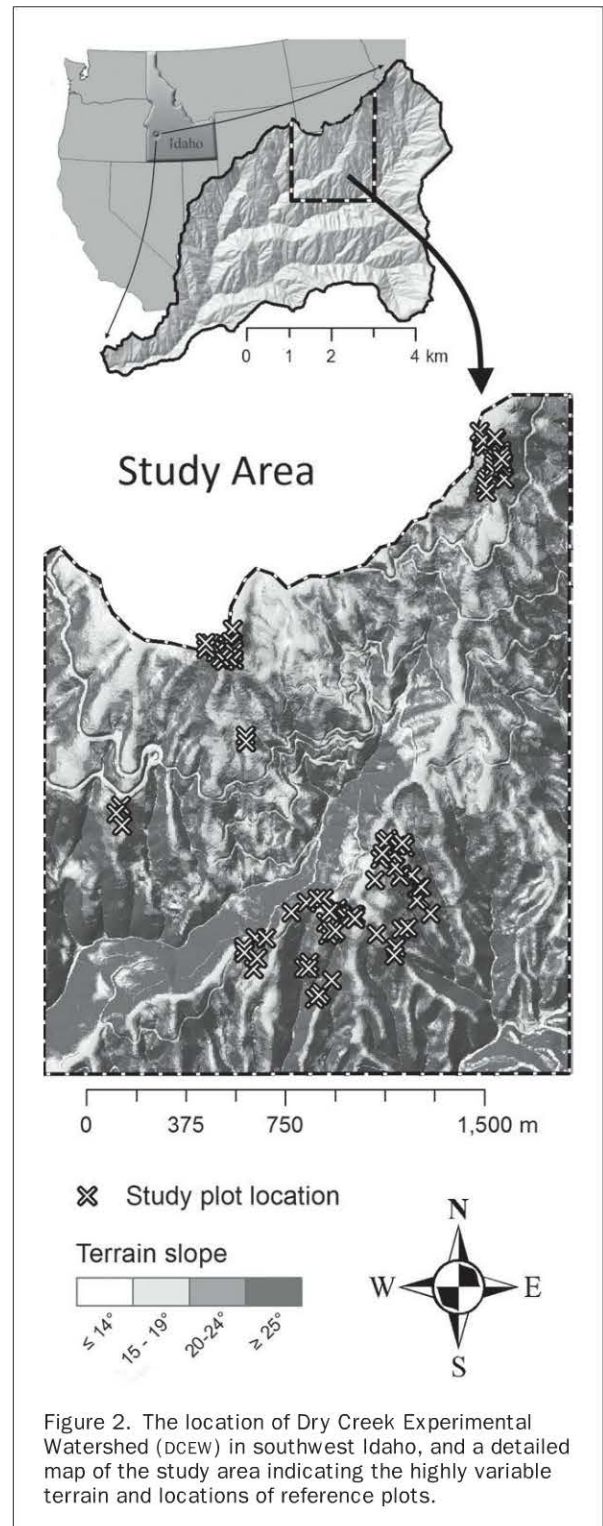

Figure 2. The location of Dry Creek Experimental Watershed (DCEW) in southwest Idaho, and a detailed map of the study area indicating the highly variable terrain and locations of reference plots.

up to four returns per laser pulse. The diameter of the laser beam when it reaches the ground (i.e., footprint) is a function of the flying height and beam divergence (0.22 mrad) and was calculated as approximately 0.20 m. Survey parameters were

set to yield an average point density of ≥4 points/m². However, the DCEW portion of the collection exceeded this baseline with average point density ranging from 4.09 to 8.68 points/m². Vendor provided field validation included 504 reference elevations surveyed on flat asphalt surfaces, returning a fundamental absolute vertical accuracy of 0.026 m RMSE. The horizontal accuracy of the data was estimated as ~1/3000th of AGL flight altitude, or ~0.30 m.

Lidar Data Processing

Lidar data were processed using Environment for Visualizing Images (ENVI) 4.8 software (Exelis Visual Information Solutions, Boulder, Colorado) and the Idaho State University's publicly available Boise Center Aerospace Laboratory (BCAL) lidar Tools[1] (Streutker and Glenn, 2006) (Figure 3). The study area encompassed multiple lidar tiles, so a 20 m horizontal buffer was applied to neighboring tiles to ensure a seamless representation in further processing. The BCAL height-filtering tool was used to classify returns as ground or vegetation. Designed for optimal use within a shrub-steppe environment, this filtering algorithm uses an iterative approach to identify ground returns. An initial search neighborhood, whose size is determined by the user and referred to as "canopy spacing" in the software tool parameters, is passed along the dataset and the lowest return in elevation within each neighborhood (canopy spacing) is classified as a ground return. A pseudo-ground surface is then interpolated from the ground returns using the selected interpolation method in the tool parameters. After the interpolation, returns that are located below the surface are classified as ground, and included in subsequent iterations. After successive iterations, all points in the dataset become classified as either ground or non-ground returns, with vegetation heights assigned to the non-ground points based on their elevation above the pseudo-ground surface. Previous studies (Glenn et al., 2011; Spaete et al., 2011) have implemented the BCAL height-filtering tool, and determined 7 m canopy spacing and natural neighbor interpolation as effective height-filtering parameters in semiarid shrub-steppe environments dominated by sagebrush and herbaceous vegetation. In contrast, the research presented herein was conducted in an ecotonal region that included sparse communities of sagebrush and grasslands, intermixed with dense populations of ceanothus. For this reason, several canopy spacing sizes (3, 5, 7, 9, and 11 m) were tested using the BCAL height-filtering tool to evaluate effectiveness of filtering and resulting DEM quality. The BCAL lidar tools were then used to create 0.5 m spatial resolution raster products (maximum vegetation-height and bare-earth) from each of the height-filtered datasets using a nearest neighbor interpolator. The maximum vegetation-height is based on the height value assigned during height-filtering, where each raster cell assumes the maximum value of all heights within each pixel. Bare-earth elevations are determined by subtracting the height value assigned during filtering from the elevation of each return. Each raster cell adopts the minimum elevation within each pixel. This technique increases the density of ground returns to help minimize interpolation error. Hereafter, the bare-earth elevation rasters will be referred to as DEMs, and subscripts indicate the size of canopy spacing used to height-filter the data. For example, DEM_{CS5} refers to a bare-earth elevation raster generated from a dataset that was height filtered using a canopy spacing of 5 m. The interpolation algorithm and cell resolution used with discrete point data influences derived DEM quality. Our selection of the nearest neighbor interpolation is based on previous research (Lloyd and Atkinson, 2002; Bater and
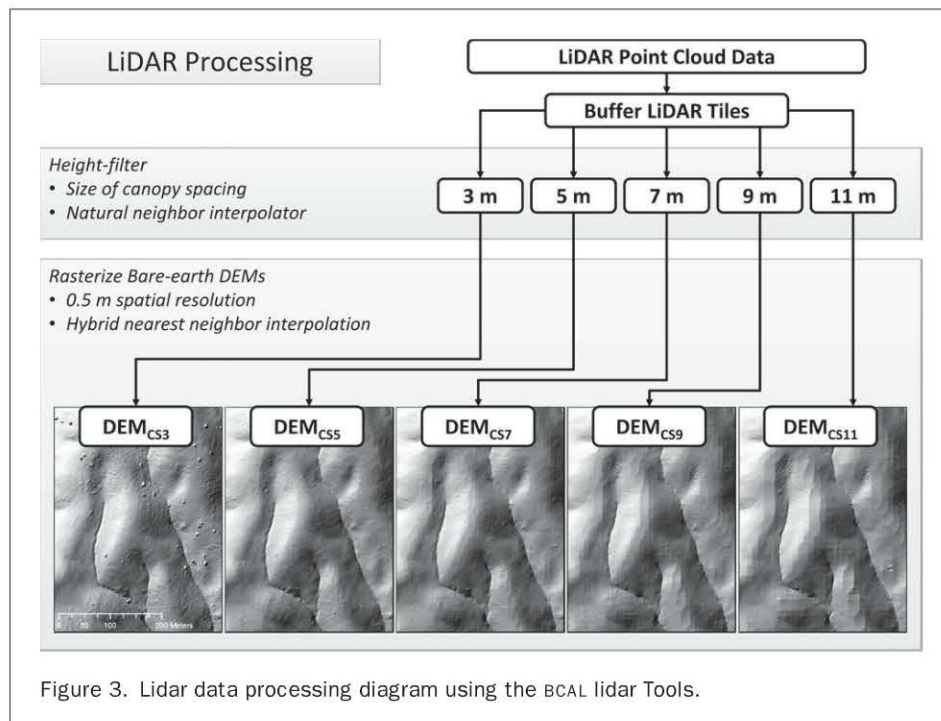

Figure 3. Lidar data processing diagram using the BCAL lidar Tools.

---

[1] URL: *http://bcal.geology.isu.edu/tools-2/envi-tools*

Coops, 2009; Guo *et al.*, 2010), suggesting less complicated interpolators (e.g., nearest neighbor) as adequate methods with negligible interpolation error when point density is high (>1 points/m²). Research has also found that the most accurate lidar-derived surfaces were created using grids that had a spacing similar to the distribution of original points (Smith *et al.*, 2004); thus, DEM resolution is constrained by the point density of the dataset (Hengl, 2006). The minimum allowable raster grid size (*s*) was calculated as 0.38 m for our dataset ($s = \sqrt{\frac{A}{n}}$, where *A* is the covered area and *n* is the number of lidar points), substantiating our use of 0.5 m raster resolution.

Field Collection
In order to evaluate DEM accuracy, an *in situ* survey was conducted in June 2011 to collect accurate ground truth data. Bare-earth elevations were surveyed at 94 reference plots, with each plot located within a uniform cover type and terrain slope (Table 1). Cover types included bare ground, where there was no vegetation, and ceanothus, which was differentiated into two separate cover categories based on two distinctly different morphological patterns. The first category, "isolated ceanothus," consisted of a single patch, distinguished by clearly defined edges and separated from surrounding shrubs. Patch sizes ranged from 5 to 30 m, as measured at the longest diameter. The second type of ceanothus, "continuous ceanothus", consisted of shrubs that had grown together to create large (> 100 m) continuous "mats" of ceanothus cover. Each ceanothus plot (isolated and continuous) was located in uniformly dense ceanothus, where there were no observable canopy gaps larger than the diameter of the lidar laser footprint (~0.20 m). Surface slopes were stratified into four classes (class 1 (≤14°), class 2 (15 to 19°), class 3 (20 to 24º), and class 4 (≥25°)); with reference plots of each cover type distributed across the four classes.

Each reference plot consisted of a single transect designed to collect an equal number of sample points at each plot (*n* = 11 per plot). In bare ground and continuous ceanothus, transects were aligned parallel to the slope of the terrain and had at least a 5 m buffer of the specified cover type. Positional coordinates and bare-earth elevations were collected at every 1 m along a 10 m transect with the first and last measurements used to calculate the average slope of the plot. At isolated ceanothus patches, transects were oriented through the longest diameter of the patch and x, y, and z coordinates were collected at equally spaced points along each transect. Additional points were collected around the perimeter of each isolated ceanothus patch and the top and bottom points were used to calculate the average slope of the plot. At each survey point within ceanothus, maximum ceanothus height was measured to the nearest 0.05 m.

A post-processed kinematic survey (Ghilani and Wolf, 2008) was implemented during field collection using Topcon GR3 survey-grade GPS receivers (Topcon Positioning, Inc., Livermore, California). Manufacturer provided accuracies[2] for the GPS receivers are sub-centimeter (3 mm +.5 ppm horizontal, 5 mm + .5 ppm vertical) for static collection, and on the order of 1 cm (1 cm + 1 ppm horizontal, 1.5 cm + 1 ppm vertical) for kinematic collection. A local reference station was not immediately available within the study area, and thus one receiver served as a base station collecting static GPS observations, while another roving-receiver collected kinematic GPS observations at the study plots. Four separate base locations were established in the study area to minimize distances

TABLE 1. DISTRIBUTION OF REFERENCE PLOTS BY SLOPE CLASS AND COVER TYPE

Slope class	Number of Reference Plots		
	Bare ground	Isolated ceanothus	Continuous ceanothus
1 (≤14°)	6	13	6
2 (15–19°)	4	11	6
3 (20–24°)	4	15	6
4 (≥25°)	3	13	7
Total (94 plots)	17	52	25

(<600 m) between the base and roving-receivers. GPS observation files collected by the base receiver were post-processed using the National Geodetic Survey's (NGS) Online Positioning User Service[3] (OPUS), and corrections were applied to the roving-receiver's GPS positions. The overall RMS values documented in the OPUS solutions were well below the NGS recommended 0.03 m, indicating high-quality solutions.

Analysis
Corresponding bare-earth elevations were extracted from each lidar-derived DEM at each reference point to assess the effect of cover type, slope category, and filtering method on DEM error. Observed elevation error was computed by subtracting the surveyed elevation from the lidar-derived elevation (ASPRS, 2004). Negative and positive values were respective indicators of underestimation and overestimation of bare-earth elevations in the lidar-derived surface. Mean signed error (MSE) and root mean square error (RMSE$_Z$) are two commonly accepted statistical measurements used to assess DEM accuracy. Several studies (Hodgson and Bresnahan, 2004; Bater and Coops, 2009; Guo *et al.*, 2010; Spaete *et al.*, 2011) have used RMSE$_Z$ values based on high-grade *in situ* surveyed elevations to determine the accuracy of DEMs across varying land-cover and topography. Hodgson and Bresnahan (2004) and Su and Bork (2006) included MSE in their analyses to identify the tendency for under- or overestimation of elevations relative to specific treatment classes. In our study, RMSE$_Z$ and MSE values were used in a similar manner and calculated for each reference plot as follows:

$$RMSE_z = \sqrt{\frac{\sum_{i=1}^{n} (Elevation_{LiDAR_i} - Elevation_{Reference_i})^2}{n}} \quad (1)$$

$$MSE = \frac{\sum_{i=1}^{n} (Elevation_{LiDAR_i} - Elevation_{Reference_i})}{n} \quad (2)$$

where $Elevation_{LiDAR_i}$ and $Elevation_{Reference_i}$ are the lidar-derived DEM and reference elevations for the ith sample point, respectively, and *n* is the number of observations per plot.

Overall mean RMSE$_Z$ was calculated for each of the DEMs by averaging all of the respective plot RMSE$_Z$ values. RMSE$_Z$ and MSE were then calculated for each cover type and slope category by averaging appropriate plot values for each of the DEMs. Analysis of variance (ANOVA) tests were performed to compare mean RMSE$_Z$ between different DEMs, cover types, and slope categories with Tamhane's T2 multiple comparisons

---

[2] URL: www.topconpositioning.com/legacy/gr-3

[3] URL: http://www.ngs.noaa.gov/OPUS/

post-hoc tests and assumptions of unequal variance (SPSS 15.0 for Windows, SPSS, Inc.). Further analysis of variance was performed to determine if any interactions existed between cover type, slope, and filtering method. Prior to all analysis, the data were examined for normality using the one-sample Kolmogorov-Smirnov test. When normality assumptions were not met, a log transform was applied to obtain a normal distribution in the data. Reference plots were categorized by cover type and grouped into subcategories based on slope. Thus, each subcategory consisted of plots with the same cover type and within the same slope class. Mean $RMSE_Z$ and MSE values were calculated for each subcategory and used to quantify expected accuracies within each of the derived DEMs.

Additional bare-earth DEMs were interpolated for each of the isolated ceanothus patches using the field-surveyed elevations (Figure 4). The resulting DEMs were used as ground reference models to analyze the proximity of returns to the ground surface. Although field-survey points had an uneven spatial distribution (around the perimeter and along a transect through the patch), the ground surface was assumed to have little variation from the local trend due to consistent slope and aspect at each plot location. It is likely that the points around the perimeter of each patch captured the local characteristics of the terrain and a trend surface prediction model was chosen for the interpolation method. A third order polynomial regression was used in the trend model to fit a least-squares surface to the input points (Childs, 2004). The Spatial Analyst extension in ArcMap® 10 (Esri, 2010) was used to interpolate the bare-earth DEMs using 0.5 m spatial resolution. Hereafter, survey-derived DEMs are annotated using a subscript and referred to as DEM_{survey}.

The vertical proximity of lidar returns to the ground surface was estimated by calculating the elevation difference between each return and its corresponding DEM_{survey}. All returns were then categorized by their proximity to the DEM_{survey} elevations using 0.15 m vertical distance intervals. The sum and cumulative percentage of all returns were calculated for each vertical distance category.

Lidar returns that were classified as "ground" during height-filtering, and located within the extent of ceanothus patches, were examined to determine their proximity to DEM_{survey} elevations using the same method described above. If the ground-classified returns (GCRs) originated from the "true" ground surface, small elevation differences between the lidar-derived DEM and DEM_{survey} would be expected. To test this assumption, differences between lidar-derived and DEM_{survey} elevations were analyzed at specific GCR locations.

Results and Discussion

Elevation Error: Cover Type

Mean plot $RMSE_Z$ varied by land-cover type and exhibited different trends depending on the DEM. ANOVA tests indicated significantly different ($p < 0.05$) $RMSE_Z$ values among cover types for DEMs derived from smaller canopy spacing (DEM_{CS3}, DEM_{CS5}, DEM_{CS7}), while $RMSE_Z$ differences among DEMs derived from larger canopy spacing (DEM_{CS9} and DEM_{CS11}) were not statistically significant ($p > 0.05$). Post-hoc multiple comparisons also indicated significant differences ($p < 0.05$) among all three cover types in DEM_{CS3} and DEM_{CS5}, with the lowest errors observed in bare ground; roughly doubling and tripling in isolated and continuous ceanothus, respectively (Figure 5). DEM_{CS7} followed a similar trend, but the differences between $RMSE_Z$ in isolated ceanothus and bare ground were not statistically significant ($p > 0.05$). Mean signed error (MSE) within each cover type appeared to decrease as the size of canopy spacing used to derive the DEM increased. DEMs with smaller canopy spacing (DEM_{CS3}, DEM_{CS5}, DEM_{CS7}) appeared to overestimate (positive MSE) bare-earth elevations in bare ground and isolated ceanothus cover type, while DEMs with larger canopy spacing (DEM_{CS9} and DEM_{CS11}) appeared to underestimate (negative MSE) bare-earth elevations (Figure 5). In the continuous ceanothus cover type, all of the derived DEMs were observed to overestimate bare-earth elevations.
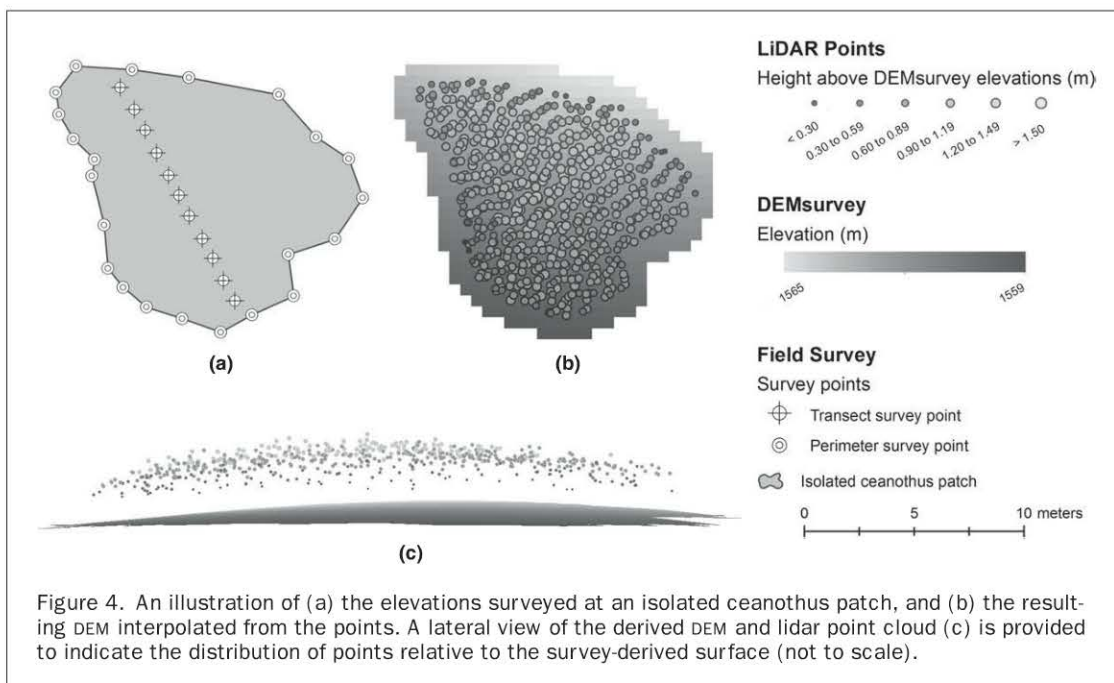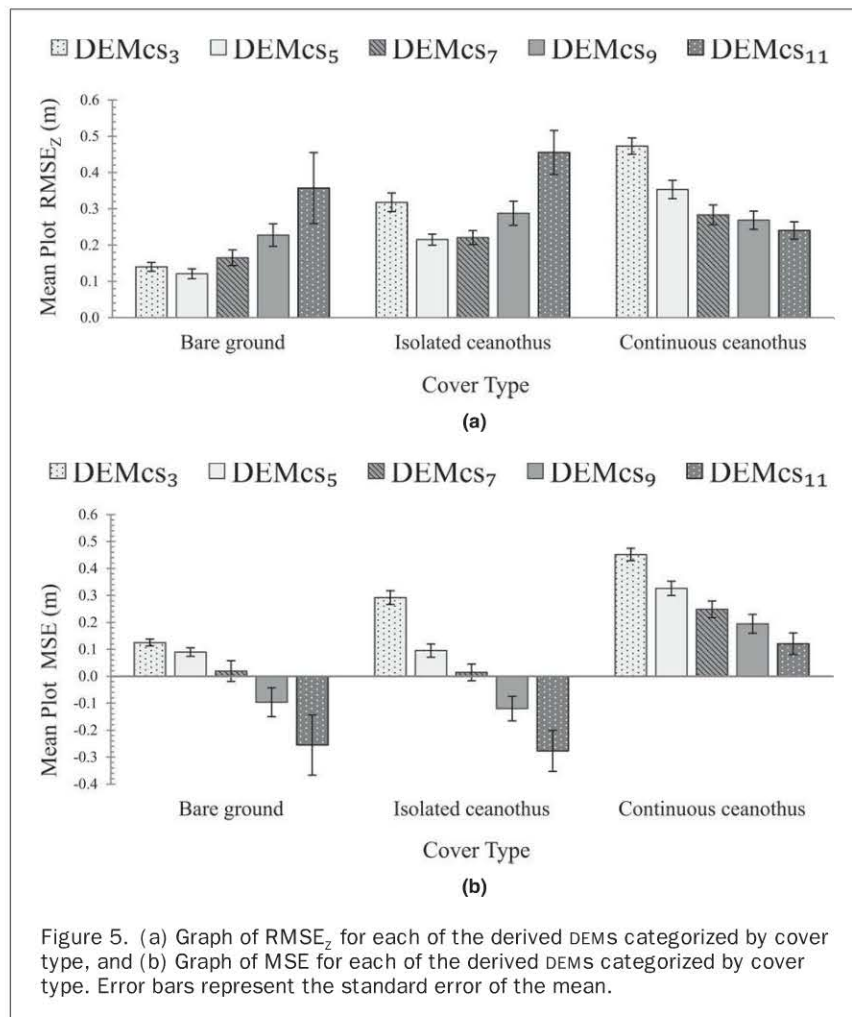

Figure 4. An illustration of (a) the elevations surveyed at an isolated ceanothus patch, and (b) the resulting DEM interpolated from the points. A lateral view of the derived DEM and lidar point cloud (c) is provided to indicate the distribution of points relative to the survey-derived surface (not to scale).

The size of canopy spacing used in the BCAL height-filtering tool influenced DEM accuracy with varying effects for each of the cover types. Since canopy spacing represents the size of the initial search neighborhood, a smaller search area is more likely to detect small changes in elevation, preserve ridges and valleys, and return a more accurate representation of the terrain. Results from the bare ground cover type support this assumption, as DEMs derived from smaller canopy spacing (DEM_{CS3}, DEM_{CS5}, and DEM_{CS7}) had smaller elevation error than those derived from larger canopy spacing (DEM_{CS9} and DEM_{CS11}) (Figure 5). In the isolated ceanothus cover type, the largest elevation errors were found in DEMs derived from both the largest (DEM_{CS11}) and smallest (DEM_{CS3}) canopy spacing (Figure 5). When the size of canopy spacing is larger than the size of a patch, a ground return from outside the patch may be identified as the "lowest" return within the search neighborhood. However, the larger search area results in a sparse distribution of ground returns, leading to an over-generalized interpolation of the bare-earth surface. On the contrary, when the size of canopy spacing is smaller than the size of a patch, it is possible for the search neighborhood to be confined within the ceanothus patch. This becomes problematic if lidar pulses fail to penetrate through the canopy and the "lowest" return is not from the ground. Subsequently mislabeled ground returns

can lead to overestimated bare-earth elevations, as evidenced by the results of DEM_{CS3} (Figure 5). We believe this assumption is transferrable to the continuous ceanothus cover type, where consistent overestimations of bare-earth elevations were found in all of the DEMs (Figure 5). The lack of open areas within the canopy coupled with canopy spacing sizes smaller than the sampled ceanothus likely led to mislabeled ground returns.

Elevation Error: Terrain Slope

Mean $RMSE_Z$ and MSE values were used to examine the influence of terrain slope on the accuracy of bare-earth elevations for each of the derived DEMs. Post-hoc comparisons indicate significant differences in mean $RMSE_Z$ among slope classes for DEM_{CS3}, DEM_{CS5}, and DEM_{CS7}. In particular, significant differences between class 1 ($\leq 14°$) and class 4 ($\geq 25°$) were found in each of the DEMs. Mean $RMSE_Z$ increased ~0.17 m from the lowest slope class to the highest for DEM_{CS3} and increased ~0.10 m for DEM_{CS5} and DEM_{CS7} (Figure 6). Results for the DEMs derived from larger canopy spacing (DEM_{CS9} and DEM_{CS11}) revealed a different trend. Although the differences were not statistically significant ($p < 0.05$), smaller errors were observed in the highest slope class compared to the lowest.
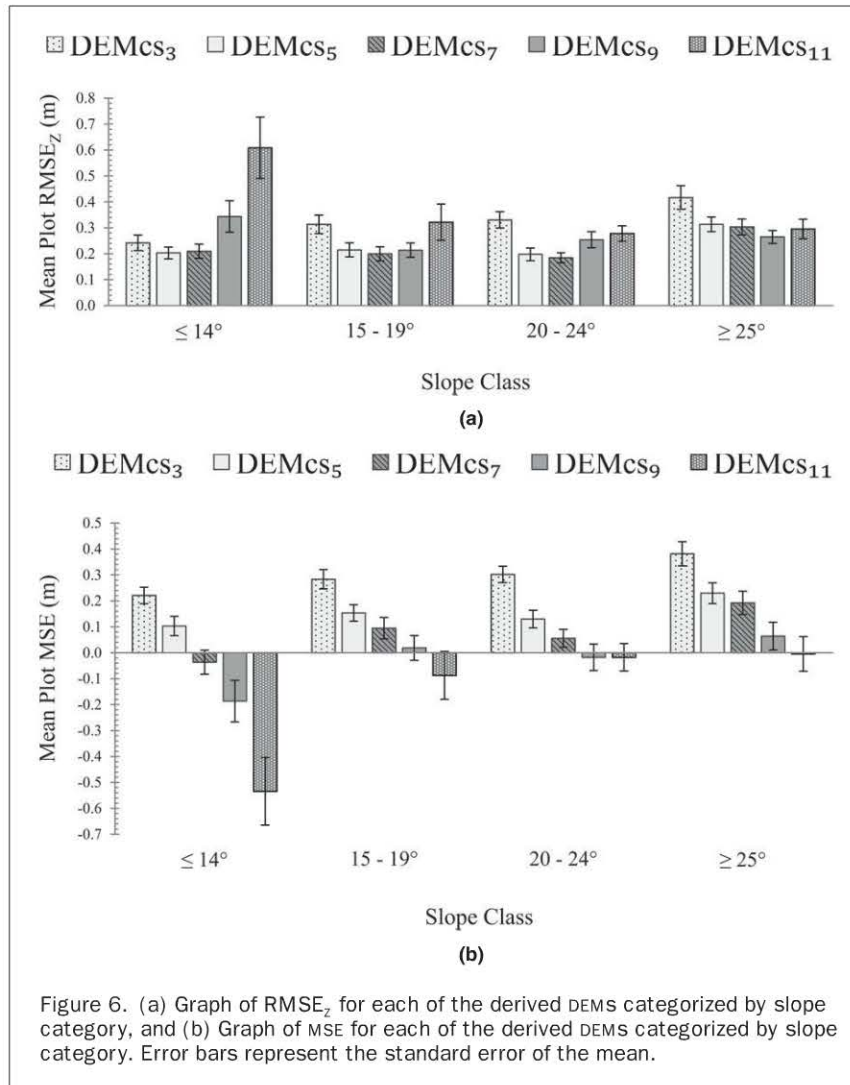

Figure 5. (a) Graph of $RMSE_Z$ for each of the derived DEMs categorized by cover type, and (b) Graph of MSE for each of the derived DEMs categorized by cover type. Error bars represent the standard error of the mean.

Figure 6. (a) Graph of RMSE$_Z$ for each of the derived DEMs categorized by slope category, and (b) Graph of MSE for each of the derived DEMs categorized by slope category. Error bars represent the standard error of the mean.

Over- and underestimations of bare-earth elevations were found in each of the slope classes (Figure 6). In slope class 1 (≤14°), DEMs using smaller canopy spacing (DEM$_{CS3}$ and DEM$_{CS5}$) appeared to overestimate bare-earth elevations, while DEMs with larger canopy spacing (DEM$_{CS7}$, DEM$_{CS9}$, and DEM$_{CS11}$) had a tendency to underestimate elevations. As terrain slope increased (slope classes 2, 3, and 4), the magnitude of overestimations appeared to increase, while the magnitude of underestimations appeared to decrease. The largest overall underestimation of bare-earth elevations was observed in slope class 1 for DEM$_{CS11}$ (−0.534 m) and the largest overestimation was observed in slope class 4 using DEM$_{CS3}$ (0.381 m).

A two-way ANOVA found the interaction between cover type and slope as not significant ($p = 0.765$), indicating that the factors were additive rather than multiplicative. The increased elevation errors at steep slopes are possibly due to error in the horizontal location of the lidar points (Maling, 1989; Hodgson and Bresnahan, 2004; Spaete et al., 2011). Potential vertical error (PVE) due to lidar horizontal error was calculated for each plot using a horizontal displacement equal to the estimated 0.30 m horizontal accuracy (Spaete et al., 2011). Plots were then stratified by slope class and average

PVE was calculated. PVE ranged from 0.043 m in the lowest slope class to 0.156 m in the highest. Although maximum PVE can only be assumed when the horizontal displacement is parallel to the surface slope, the increased PVE at high slopes may have contributed to the observed elevation errors.

Quantifying DEM Accuracy
The variability in DEM error made it unreasonable to make a generalized quantification of DEM accuracy without considering all of the potential factors. For example, an area where isolated ceanothus was present and the terrain slope was ~15°, estimated accuracy for DEM$_{CS7}$ was ~0.20 m (RMSE$_Z$). When data for the same area were processed using 11 m canopy spacing, the predicted accuracy was considerably higher (0.41 m RMSE$_Z$). Thus, reference plots were grouped by cover type and within those groupings, differentiated by slope class. DEM accuracy (mean RMSE$_Z$ and MSE) was calculated for each combination of cover type and slope class (Table 2). The RMSE$_Z$ may be used as an expected level of accuracy and the MSE indicates the tendency for over- or underestimation of bare-earth elevations.

Cover type	Slope class	DEM$_{CS3}$		DEM$_{CS5}$		DEM$_{CS7}$		DEM$_{CS9}$		DEM$_{CS11}$	
		RMSE$_z$	MSE	RMSE$_z$	MSE	RMSE$_z$	MSE	RMSE$_z$	MSE	RMSE$_z$	MSE
Bare ground	1 (≤ 14°)	0.126	0.120	0.106	0.085	0.186	−0.043	0.253	−0.150	0.605	−0.544
	2 (15°–19°)	0.118	0.094	0.103	0.073	0.106	−0.002	0.221	−0.136	0.235	−0.199
	3 (20°–24°)	0.128	0.096	0.102	0.057	0.136	−0.010	0.209	−0.112	0.227	−0.141
	4 (≥ 25°)	0.212	0.184	0.200	0.167	0.240	0.211	0.209	0.086	0.197	0.097
Isolated ceanothus	1 (≤ 14°)	0.207	0.176	0.190	0.014	0.222	−0.129	0.426	−0.349	0.802	−0.765
	2 (15°–19°)	0.342	0.307	0.208	0.117	0.201	0.052	0.211	−0.016	0.415	−0.162
	3 (20°–24°)	0.331	0.300	0.178	0.088	0.170	0.016	0.250	−0.081	0.285	−0.038
	4 (≥ 25°)	0.385	0.343	0.274	0.155	0.278	0.109	0.257	-0.031	0.332	−0.144
Continuous ceanothus	1 (≤ 14°)	0.433	0.419	0.329	0.313	0.205	0.170	0.256	0.129	0.193	−0.025
	2 (15°–19°)	0.391	0.368	0.301	0.274	0.259	0.236	0.213	0.185	0.207	0.124
	3 (20°–24°)	0.492	0.471	0.324	0.295	0.260	0.210	0.300	0.222	0.299	0.135
	4 (≥ 25°)	0.552	0.527	0.429	0.394	0.374	0.341	0.300	0.234	0.264	0.219

Distribution of Lidar Returns in Ceanothus Canopy

Lidar returns within isolated ceanothus patches were examined to determine their proximity to the DEM$_{survey}$ elevations. It was hypothesized that returns with small differences in elevation (<0.15 m) from the DEM$_{survey}$ had a high potential of being ground returns. Results found only 5 of the total (15,703) returns with elevations that were equal to the DEM$_{survey}$ elevations and 149 returns with elevation difference ≤0.15 m (Table 3). The finding of a small percentage of returns with elevations close to DEM$_{survey}$ elevations supports the assumption that few laser pulses can penetrate through the ceanothus canopy and return accurate bare-earth elevations. It is also notable that of the 149 returns with elevation differences <0.15 m, over 100 of the returns were found within a single ceanothus patch. Further examination revealed that nearly all of these returns were located at the edge of the patch, and we speculate that they originated from the ground surface outside of the patch. We conclude that within the majority of patches there were no lidar returns that originated from the ground surface.

Relationship Between GCRs and Elevation Error

GCRs were investigated using the same criteria mentioned above to determine their proximity to the ground surface, and only ten GCRs were found within a 0.15 m of the DEM$_{survey}$ elevations (Table 3). Further exploration of the GCRs exposed substantial deviations from the DEM$_{survey}$ elevations. Over half of the GCRs had elevations >0.30 m higher than the DEM$_{survey}$ elevations (Table 3). These discrepancies are intriguing and suggest that returns were likely mislabeled during the height-filtering process. Furthermore, a strong tendency was found for overestimation of lidar-derived elevations at specific GCR locations. Previous research (Raber et al., 2007; Hodgson and Bresnahan, 2004) determined that a higher density of ground returns correlate with greater DEM accuracy. Undoubtedly, those conclusions were based on the assumption that the ground returns were accurate representations of bare-earth elevations. Our study concludes that the high elevation errors at GCR locations are attributed

to mislabeled returns, which originated from within the ceanothus canopy. Therefore, the higher density of mislabeled ground returns would lead to a greater overestimation of the ground surface.

An optional parameter in the BCAL height-filtering tool allows for the user to input a ground threshold value that consequently identifies more GCRs. Additional height-filtering was performed using a 0.15 m threshold value, resulting in all points within 0.15 m of the original identified ground surface to be included in the ground classification. Although the number of GCRs increased to 264, the proximity of the returns to the DEM$_{survey}$ elevations followed a similar distribution as the method where no threshold was used. Roughly half of the GCRs (130) had elevations >0.30 m higher than the DEM$_{survey}$ elevations. Both methods provided similar elevation errors, indicating that the increased number of ground returns using the threshold were likely subject to the same mislabeling error and failed to provide a more accurate DEM.

Impact on Estimated Ceanothus Heights

A direct point-based comparison between the 535 field-measured ceanothus heights and corresponding lidar-derived heights revealed an accuracy of 0.28 m (RMSE$_z$). Although the error appears to be relatively small, 0.28 m represents a substantial fraction (~one-third) of the average height of ceanothus (0.85 m). These results are consistent with other studies that have found similar height errors using lidar data in low-height vegetation such as sagebrush (Glenn et al., 2011; Mitchell et al., 2011). Lidar also had a slight overall tendency to underestimate heights (MSE = -0.026 m), but examination of the specific errors showed a wide range (-0.93 to 0.63 m) of both over- and under-predicted heights. Furthermore, errors were variable even within a single ceanothus patch, and simple linear regression showed DEM elevation error as a significant predictor variable ($p < 0.001$, $R^2 = 0.434$) for ceanothus height error. Where ground elevations were overestimated, ceanothus heights were underestimated, and vice versa. This highlights the importance of an accurate bare-earth DEM as errors will propagate into further lidar-derived products.

Table 3. Vertical Distribution of All Lidar Returns and Only Ground Classified Returns (GCRs) within Isolated Ceanothus Patches

Height above DEMsurvey elevations (m)	All lidar Returns			Ground Classified Returns (GCRs)		
	No. of Returns	% of All Returns	Cumulative % of Returns	No. of GCRs	% of All Returns	Cumulative % Of GCRs
0.00	5	0.03%	0.03%	0	0.00%	0.00%
0.01 to 0.15	149	0.95%	0.98%	10	0.06%	13.51%
0.16 to 0.30	377	2.40%	3.38%	23	0.15%	44.59%
0.31 to 0.45	811	5.16%	8.55%	14	0.09%	63.51%
0.46 to 0.60	1825	11.62%	20.17%	9	0.06%	75.68%
0.61 to 0.75	2708	17.25%	37.41%	8	0.05%	86.49%
0.76 to 0.90	3168	20.17%	57.59%	3	0.02%	90.54%
0.91 to 1.05	2965	18.88%	76.47%	3	0.02%	94.59%
1.06 to 1.20	1999	12.73%	89.20%	1	0.01%	95.95%
1.21 to 1.35	1016	6.47%	95.67%	3	0.02%	100.00%
1.36 to 1.50	453	2.88%	98.55%	n/a	n/a	n/a
1.51 to 1.65	170	1.08%	99.64%	n/a	n/a	n/a
1.66 to 1.80	49	0.31%	99.95%	n/a	n/a	n/a
1.81 to 1.95	7	0.04%	99.99%	n/a	n/a	n/a
1.96 to 2.10	1	0.01%	100.00%	n/a	n/a	n/a

Implications of Height-filtering

The height-filtering method is another potential source of error as highly varying terrain and low vegetation are challenging for automated filtering processes (Sithole and Vosselman, 2004). The first iteration of our height-filtering method identifies ground returns as the lowest lidar return within a specified neighborhood (canopy spacing). In steep sloping terrain, it is possible for a return in the vegetation canopy to have a lower elevation than a ground return if it is located downslope. The resulting mislabeled ground returns may have contributed to the observed DEM errors in our study. It is emphasized, however, that an accurately filtered dataset would still lack ground returns beneath dense vegetation cover, and the determination of bare-earth elevations would be contingent on interpolation from neighboring ground returns.

Conclusions

Investigating errors in lidar-derived bare-earth DEMs is critical for understanding the accuracy of lidar and derived products when applied to studies of the natural environment. The research presented here extends previous assessments of DEM accuracy by examining errors introduced by a specific shrub species in a complex mountainous environment. Findings are consistent with other studies (Hodgson *et al.,* 2003; Hodgson and Bresnahan, 2004) that found signed elevation errors were high in the shrub vegetation compared with other vegetation. Although the magnitude of errors varied by ceanothus cover type (isolated or continuous), slope, and height-filtering parameters, we conclude that errors were largely attributable to the tendency of ceanothus to obstruct lidar pulse penetration due to its dense stand characteristics and leaf structure. Fewer than half of the ground classified returns in our study had elevations within 0.30 m of the DEMsurvey elevations, suggesting that several of the ground classified returns were mislabeled during height-filtering and led to elevation errors in derived DEMs. These findings are significant because they not only highlight the importance of understanding the filtering process, but also demonstrate the difficulty in generating an accurate bare-earth model when "true" ground returns are not available in the dataset due to high density vegetation cover. Therefore, users should be aware of potential introduced errors and consider the accuracy of lidar-derived DEMs in the context of specific vegetation types when applying the models to studies of the natural environment.

The development of improved vegetation filtering methods continues to be an active area of research with a necessary focus on surfaces with rough terrain and low vegetation (Meng 2010). Briese (2010) acknowledges that a common deficiency in many filtering algorithms is that they focus on the geometric relationship between points in a local neighborhood and that the bare earth cannot be characterized in certain areas by geometric means alone. A new generation of full-waveform airborne lidar systems may be able to provide radiometric information from the complete backscattered waveform to discriminate low vegetation from ground reflections (Briese, 2010). As an example, Doneus and Briese (2006) implemented a pre-filter step to eliminate low vegetation based on echo width, which led to a significant improvement in DEM quality.

While this research was demonstrated in a specific study location, the findings are applicable and important in the larger region due to the wide distribution of ceanothus and its sub-species in several mountainous ecosystems throughout the western US and Canada. Furthermore, it is reasonable to conclude that unrelated species with similar characteristics (e.g., broadleaf evergreen shrubs) likely interact with lidar in much the same manner. This is consistent with conclusions from previous studies in the chaparral ecosystem of southern California (Cooke, 2008) that attributed elevation errors to the dense vegetation which provided few canopy gaps through which the lidar pulses could penetrate.

References

Aishlin, P., and J.P. McNamara, 2011. Bedrock infiltration and mountain block recharge accounting using chloride mass balance, *Hydrological Processes*, 25:1934–1948.

Anderson, M.D., 2001. Ceanothus velutinus, Fire Effects Information System, URL: *http://www.fs.fed.us/database/feis/plants/shrub/ceavel/all.html*, US Department of Agriculture, Forest Service, Rocky Mountain Research Station, Fire Sciences Laboratory (last date accessed: 08 February 2013).

American Society for Photogrammetry and Remote Sensing Lidar Committee, 2004, *ASPRS Guidelines: Vertical Accuracy Reporting for Lidar Data*, Bethesda, Maryland.

Baltsavias, E.P., 1999. Airborne laser scanning: Existing systems and firms and other resources, *ISPRS Journal of Photogrammetry and Remote Sensing*, 54:164–198.

Bater, C.W., and N.C. Coops, 2009. Evaluating error associated with lidar-derived DEM interpolation, *Computers & Geosciences*, 35:289–300.

Beraldin, J.A., Blais, F., and U. Lohr, 2010. Laser scanning technology, *Airborne and Terrestrial Laser Scanning*, Whittles Publishing, Boca Raton, Florida, pp. 1–44

Briese, C., 2010. Extraction of digital terrain models, *Airborne and Terrestrial Laser Scanning*, Whittles Publishing, Boca Raton, Florida, pp. 135–167

Cooke, A.G., 2008. *Analysis of LiDAR-derived bare ground model accuracy in southern California chaparral*, Master's Thesis, University of Washington, Seattle, Washington, 113 p.

Doneus, M., and C. Briese, 2006. Digital terrain modelling for archaeological interpretation within forested areas using full-waveform laserscanning, *Proceedings of the 7th International Symposium on Virtual Reality, Archaeology and Cultural Heritage VAST* (M. Ioannides, D. Arnold, F. Niccolucci, and K. Mania, editors), Eurographics Association, Aire-la-Ville, pp. 155–162.

Forlani, G., and C. Nardinocchi, 2007. Adaptive filtering of aerial laser scanning data, *Proceedings of the ISPRS Workshop on Laser Scanning 2007 and SilviLaser 2007*, 12–14 September, Espoo, Finland, pp. 130–135.

Ghilani, C.D., and P.R. Wolf, 2008. *Elementary Surveying: An Introduction to Geomatics*, Pearson Education, Inc., Upper Saddle River, New Jersey, 886 p.

Glenn, N.F, L.P. Spaete, T.T. Sankey, D.R. Derryberry, S.P. Hardegree, and J.J. Mitchell, 2011. Errors in LiDAR-derived shrub height and crown area on sloped terrain, *Journal of Arid Environments*, 75(4):377–382.

Guo, Q., L. Wenkal, H. Yu, and O. Alvarez, 2010. Effects of topographic variability and lidar sampling density on several DEM interpolation methods, *Photogrammetric Engineering & Remote Sensing*, 76(6):1–12.

Hengl, T., 2006. Finding the right pixel size, *Computer and Geosciences*, 32(9):1283-1289.

Hodgson, M.E., and P. Bresnahan, 2004. Accuracy of airborne Lidar-derived elevation: Empirical assessment and error budget, *Photogrammetric Engineering & Remote Sensing*, 70(3):331–339.

Lilliefors, H.W., 1967. On the Kolmogorov-Smirnov test for normality with mean and variance unknown, *Journal of the American Statistical Association*, 62(318):399–402.

Liu, X., 2008. Airborne LiDAR for DEM generation: Some critical issues, *Progress in Physical Geography*, 32(1):31–49.

Lloyd, C., and P. Atkinson, 2002. Deriving DSMs from LiDAR data with kriging, *International Journal of Remote Sensing*, 23(12):2519–2524.

Maling, D.H., 1989. *Measurements from Maps*, Pergamon Press, New York, 577 p.

McNamara, J.P., D.G. Chandler, M. Seyfried, and S. Achet, 2005. Soil moisture states, lateral flow, and streamflow generation in a semi-arid, snowmelt-driven catchment, *Hydrological Processes*, 19:4023–4038.

Meng, X., N. Currit, and K. Zhao, 2010. Ground filtering algorithms for airborne LiDAR data: A review of critical issues, *Remote Sensing*, 2:833–860.

Mitchell, J.J., N.F. Glenn, T.T. Sankey, D.R. Derryberry, M.O. Anderson, and R.C. Hruska, 2011. Small-footprint lidar estimations of sagebrush canopy characteristics, *Photogrammetric Engineering & Remote Sensing*, 77(5):521–530.

Raber, G.T., J.R. Jensen, M.E. Hodgson, J.A. Tullis, B.A. Davis, and J. Berglund, 2007. Impact of lidar nominal post-spacing on DEM accuracy and flood zone delineation, *Photogrammetric Engineering & Remote Sensing*, 73(7):793–804.

Reutebuch, S.E., R.J. McGaughey, H.E. Andersen, and W.W. Carson, 2003. Accuracy of a high-resolution LiDAR terrain model under a conifer forest canopy, *Canadian Journal of Remote Sensing*, 29:527–535.

Sankey, T.T., and P. Bond, 2011. LiDAR-based classification of sagebrush community types, *Rangeland Ecology and Management*, 64:92–98.

Schmid, K.A., B.C. Hadley, and N. Wijekoon, 2011. Vertical accuracy and use of topographic LiDAR data in coastal marshes, *Journal of Coastal Research*, 27(6A):116–132.

Shallcross, A.T., 2011. *LiDAR Investigations of Snow Distribution in Mountainous Terrain*, Master's Thesis, Boise State University, Boise, Idaho, 61 p.

Sithole, G., and G. Vosselman, 2004. Experimental comparison of filter algorithms for bare-earth extraction from airborne laser scanning point clouds, *ISPRS Journal of Photogrammetry & Remote Sensing*, 59:85–101.

Smith, S., D. Holland, and P. Longley, 2004. The importance of understanding error in lidar digital elevation models, *International Archives of Photogrammetry, Remote Sensing and Spatial Information Sciences*, 35:996–1001.

Spaete, L.P., N.F. Glenn, D.R. Derryberry, T.T. Sankey, J.J. Mitchell, and S.P. Hardegree, 2011. Vegetation and slope effects on accuracy of a LiDAR-derived DEM in the sagebrush steppe, *Remote Sensing Letters*, 2(4):317–326.

Streutker, D.R., and N.F. Glenn, 2006. LiDAR measurement of sagebrush steppe vegetation heights, *Remote Sensing of Environment*, 102:135–145.

Su, J., and E. Bork, 2006. Influence of Vegetation, Slope, and Lidar Sampling Angle on DEM Accuracy, *Photogrammetric Engineering & Remote Sensing*, 72(11):1265–1274.

Williams, C., 2005. *Characterization of the Spatial and Temporal Controls on Soil Moisture and Streamflow Generation in a Semi-arid Headwater Catchment*, Master's Thesis, Boise State University, Boise, Idaho.

Zavitkovski, J., and M. Newton, 1968. Ecological importance of snowbrush, *Ceanothus velutinus*, in the Oregon Cascades, *Ecology*, 49(6):1136–1137.